Influence of Onion-like Carbonaceous Particles on the Aggregation Process of Hydrocarbons

Xiaoqi Zhou, Zhisen Meng, Sylvain Picaud, Michel Devel, Jesús Carrete, Georg Madsen, Yulu Zhou, Zhao Wang

ACS OMEGA

http://pubs.acs.org/journal/acsodf

Article

Influence of Onion-like Carbonaceous Particles on the Aggregation Process of Hydrocarbons

Xiaoqi Zhou, Zhisen Meng, Sylvain Picaud, Michel Devel, Jesús Carrete, Georg K. H. Madsen, Yulu Zhou,* and Zhao Wang

Cite This: *ACS Omega* 2021, 6, 27898−27904

Read Online

ACCESS | Metrics & More | Article Recommendations | Supporting Information

ABSTRACT: Molecular dynamics simulations are performed to characterize the nucleation behavior of organic compounds in the gas phase. Six basic molecular species are considered—ethylene, propylene, toluene, styrene, ethylbenzene, and *para*-xylene—in interaction with onion-like carbon nanostructures that model soot nanoparticles (NPs) at room temperature. We identify a shell-to-island aggregation process during the physisorption of aromatic molecules on the soot surface: The molecules tend to first cover the NP in a shell, on top of which additional adsorbates form island-shaped aggregates. We present results for the binding energy, suggesting that the NPs lead to the formation of more stable molecular aggregates in comparison with the pure gas phase. Our findings describe a plausible microscopic mechanism for the active role of soot in the formation and growth of organic particulate matter.

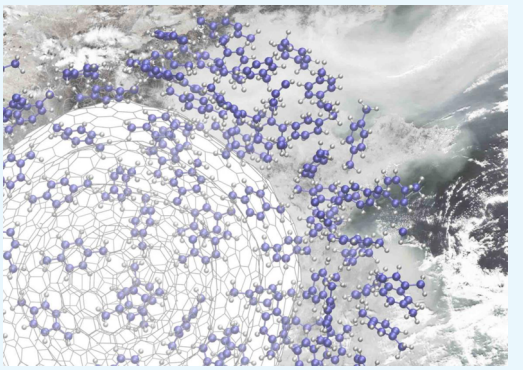

INTRODUCTION

Soot-based particulate matter (soot-PM) takes part in many environmental processes that impact climate and health. Its formation has been the focus of many experimental studies.[1] Transmission electron microscopy observations revealed that soot-PM are frequently in the form of carbon nanoparticles (NPs) enveloped by organic coverings.[2,3] Organic compounds from diverse environmental sources were reported to act as precursors in the condensation of soot-PM.[4−6] New particle formation occurs in two distinct stages, nucleation to form a critical nucleus and subsequent growth of the critical nucleus to a larger size.[7,8] However, the kinetic physicochemical processes at the root of the formation of soot-PM are unclear, particularly the molecular nucleation involving the physisorption of organic compounds on soot NPs.

Low-dimensional carbons have drawn considerable attention for molecular adsorption, thanks to their chemical inertness and peculiar structures. On the basis of density functional theory calculations, Lazar *et al.* reported that the static adsorption enthalpy of acetone, toluene, or hexane on graphene flakes ranges from 7.0 to 15.0 kcal/mol depending on the molecular species and the degree of the surface coverage.[9] It was suggested that stable molecular aggregates of hydrocarbons could form on graphitic surfaces (such as the soot surface) *via* physisorption. On the basis of MD simulations, Veclani and Melchior studied the adsorption of neutral and zwitterionic forms of ciprofloxacin on single-walled carbon nanotubes in the gas phase and water. They found that the adsorbed molecules oriented parallel to the surface interacting *via* $\pi-\pi$ interactions.[10] Yang *et al.* systematically studied the adsorption of polycyclic aromatic hydrocarbons (PAHs) on various carbon nanomaterials. For different PAHs, adsorption seemed to relate with their molecular size, that is, the larger the molecular size, the lower the adsorbed volume capacity.[11] In contrast, little is known about the kinetic adsorption process on soot. For example, about how the shape and the energetics of the molecular clusters change with different types of adsorbates during the growth of soot-PM.

There has been a great amount of experimental research on the adsorption of aliphatic and aromatic molecules on different adsorbents. For the alkenes, the adsorption capacity of C_3H_6 was higher than that of C_2H_4 for most of the adsorbents.[12] The adsorption of BTEX on activated carbon was observed to proceed in the order xylene > ethylbenzene > toluene > benzene, as related to decreased solubility and increased molecular weight.[13] It is also reported that carbon nanotubes have higher adsorption affinities for the organic compounds with a planar molecular configuration.[14,15] The nucleation of organic molecules was often studied with MD simulations.[16−18] We here used MD to simulate the physisorption of simple hydrocarbon molecules on the surface of carbon NPs in order to gain physicochemical insights into the formation of soot-PM. We selected six common carbohydrates due to their

Received: July 7, 2021
Accepted: September 29, 2021
Published: October 14, 2021

simple but diverse structures. The set comprises two aliphatic compounds, namely ethylene and propylene, and four aromatic ones, namely toluene, styrene, ethylbenzene, and *para*-xylene, as shown in the left panel of Figure 1. The nucleation of these molecules in their pure gas phase was also simulated to establish a baseline for comparison.

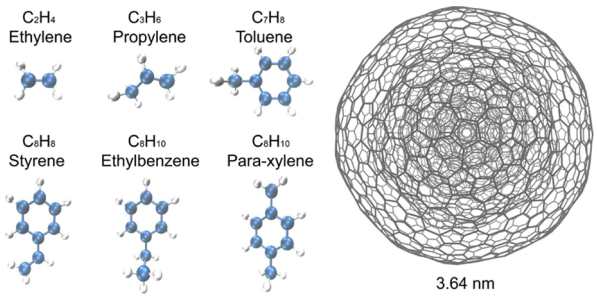

Figure 1. Structures and chemical formulas of the six organic compounds studied in this work. In the ball-and-stick model, carbon atoms are depicted in blue and hydrogen atoms in gray. The NP (of diameter 3.64 nm) used to model soot is also shown on the right-hand side of the figure.

COMPUTATIONAL METHODS

The geometry of our model soot NPs is based on experimental reports of onion-like carbon nanostructures characterized by means of spectrometry and electron microscopy.[19−21] To mimic that kind of morphology, we built a bucky onion that contains a number of concentric fullerene layers, as shown in the right panel of Figure 1. We had to use relatively small soot NPs due to the limitation of our computational resources. We have therefore studied two systems of different sizes to see the size effect. Four and six concentric fullerene layers have been used to construct the soot particles of 3.64 and 4.58 nm, respectively. The quasi-spherical fullerenes are constructed by introducing Stone−Wales defects on the edges or medians of each triangle containing a pentagon at its vertices of the icosahedral or triacontahedral fullerenes using the method introduced in ref 22. We note that our model is a simplification because more complex morphologies of the soot monomer were reported. For example, a soot monomer was observed to exhibit an amorphous carbon core surrounded by a shell of crystalline graphite plates.[23] The choice of the six organic compounds is based on their abundance that dominates the atmospheric pollution in modern cities.[24,25] We have selected only hydrocarbons in this work for simplifying the computations.

We used the parallel MD package LAMMPS[26] for our simulations. The interaction potential energies and forces were computed using the adaptive interatomic reactive empirical bond order (AIREBO) force field. The total energy is a collection of the contributions from individual bonds, which are functions of many-body interactions. The van der Waals interactions between the NP and the molecules, between the NP layers, and between the molecules are included in AIREBO using a parametrized long-range Lennard-Jones function with a cutoff radius of 1.0 nm. Details about the formulation, the parameters, and the benchmark calculation of this force field are provided elsewhere.[27] We chose AIREBO because of its inclusion of bond rotation and torsion terms that are important for taking into account the deformation of the substrate caused by adsorbates and thermal fluctuation,[28] which has been reported to influence gas adsorption.[29] AIREBO is a widely used force field for hydrocarbon systems because it allows the breaking or the formation of chemical bonds that could occur between the molecules and the substrate. However, we did not observe any expected chemisorption in our simulations, probably because the studied temperature is relatively low.

At the beginning of the simulation, a specified number of organic molecules are placed at random sites near the surface of the NP in a periodic simulation cell of $10 \times 10 \times 10$ nm^3. In atmospheric conditions, the nucleation time is orders of magnitude longer than that can be treated by MD. It is a common MD approach to increase the molecular density for accelerating the process. Because of this simplification, we simulated different numbers of molecules and tried to understand the effect of molecular density on the adsorption behavior (Figure 2). Initial velocities are sampled from the Maxwell−Boltzmann distribution, and then, a Langevin thermostat is used with a friction coefficient in the Langevin

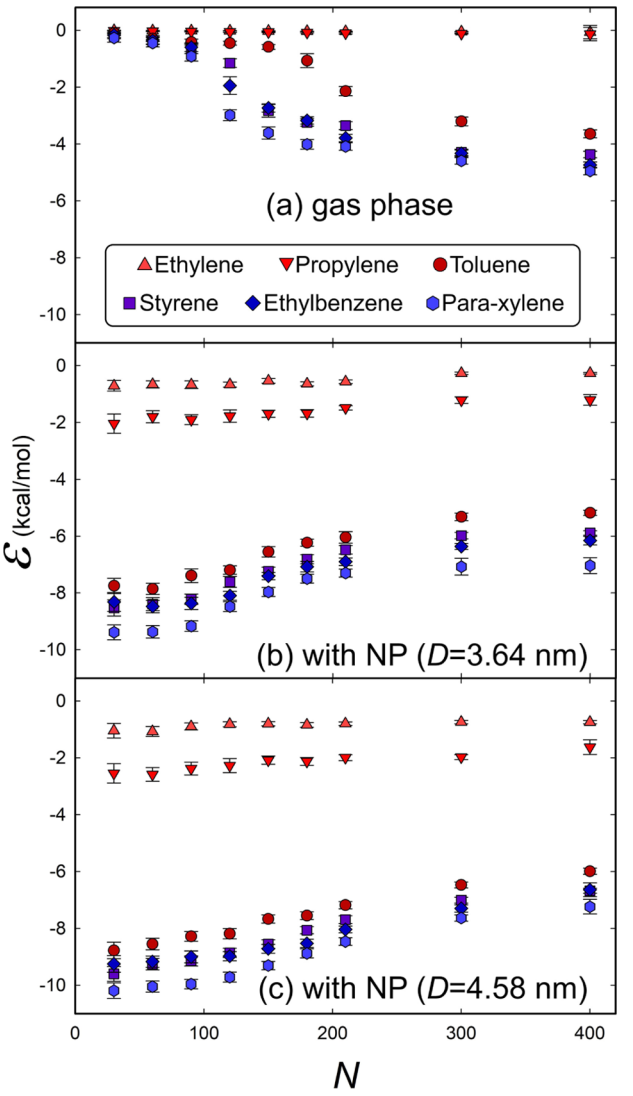

Figure 2. Binding energy per molecule *vs* the number of molecules for different molecular species in the gas phase without any NP (a) or on the surface of an NP with a diameter of 3.64 (b) or 4.58 nm (c). The data are averaged over the last 1000 frames of simulation for 0.5 ns. The error bars show the standard deviation.

https://doi.org/10.1021/acsomega.1c03571
ACS Omega 2021, 6, 27898−27904

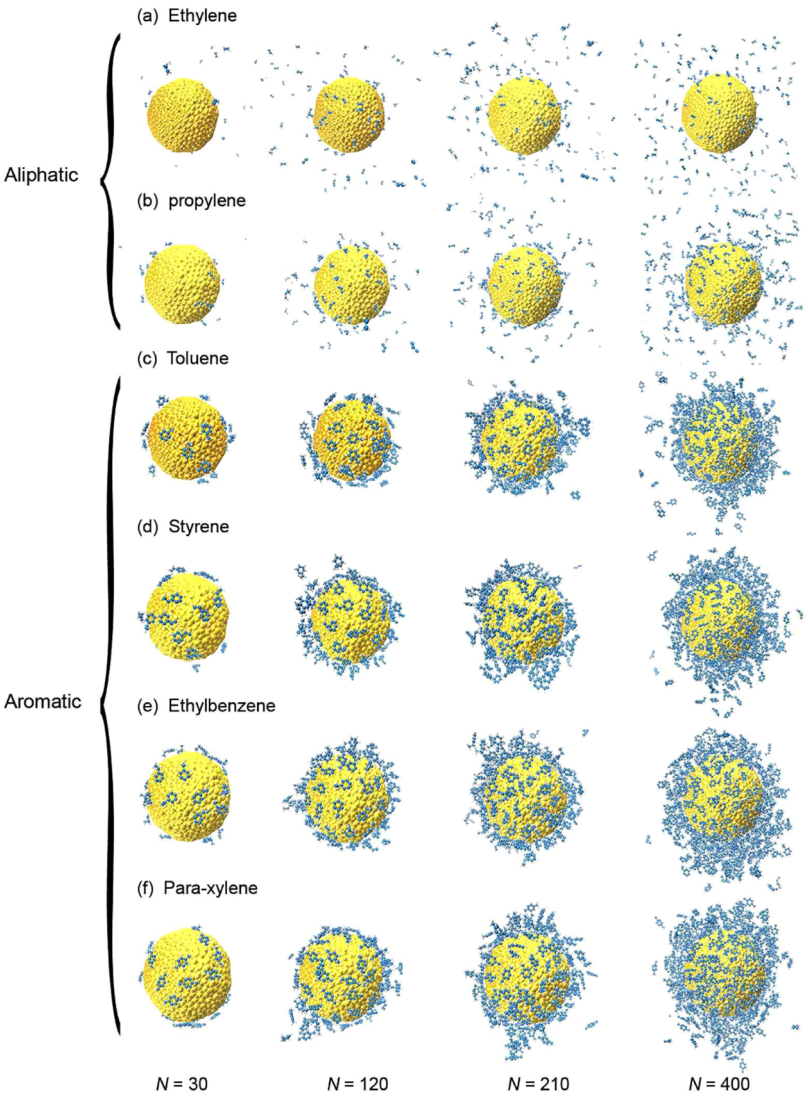

Figure 3. Atomistic configurations of different numbers of (a) ethylene, (b) propylene, (c) toluene, (d) styrene, (e) ethylbenzene, and (f) *para*-xylene molecules on an NP.

equation corresponding to a coupling time of 0.05 ns for a period of 2.5 ns to let the NP progressively reach thermal equilibrium at 300 K. The simulation timestep is 0.0005 ps. The damping constant is 100 ps. The simulation duration is determined by a set of convergence tests, as shown in the Supporting Information. The gas phase (without NP) is also simulated under the same conditions for comparison, except that the thermostat is applied directly to the organic molecules instead of to the NP. We used different thermostats for the gas phase than in the case of NPs in order to reduce the simulation artifact. In the case of NPs, the molecules are set to be free, and their temperature is controlled by energy exchange with NPs. The NPT ensemble has to be applied for the pure gas phase. The simulations are still run for 0.5 ns after reaching thermal equilibrium for computing the binding energy. The total time of simulations is 3 ns for each system. The binding energy is computed at an interval of 0.5 ps where each coordination frame is saved and is averaged over 1000 points for a period of 0.5 ns after reaching thermal equilibrium. This work considers densities higher than those in real conditions because of the limitation of the simulation time. However, because the relaxation time is long enough to ensure that the system equilibrium is reached, the simulation can still provide microscopic insights into the adsorption process.

RESULTS AND DISCUSSION

We computed the binding energy per molecule ε, a key variable associated with the nucleation of gaseous compounds that indicates how easy or difficult it is for the molecules to form aggregates, as

$$\varepsilon = \frac{\varepsilon^{\text{total}} - (\varepsilon^{\text{np}} + \sum_{i=1}^{N} \varepsilon_i^{\text{a}})}{N} \quad (1)$$

where $\varepsilon^{\text{total}}$ is the total interaction energy of the system, ε^{a} is the internal energy of the individual molecule, and ε^{np} is the internal energy of the NP (or simply zero if no NP is present, *i.e.*, in the gas phase). As shown in Figure 2, we plot ε versus the number of molecules N in the gas phase (a) and in the presence of NPs (b and c). ε is of the same order of magnitude as those reported in a previous study of organic molecules adsorbed on graphene.[9] By comparing the vertical axis of the panels of Figure 2, it was observed that ε is, in general, lower for the two cases where NPs are present, suggesting that the

https://doi.org/10.1021/acsomega.1c03571
ACS Omega 2021, 6, 27898−27904

clusters formed on the NP surface are more stable than the ones formed in the gas phase. These results could be correlated with the formation of the previously reported morphology of soot PM with organic coverings[4−6] and indicate an active role of soot as an effective substrate for facilitating the initial growth of organic PM, a hypothesis also supported by the experimentally measured positive correlations between the concentrations of organic aerosols and soot (also called black carbon).[30−35]

It is well known that the nucleation of aromatic compounds is different from that of aliphatic compounds;[36] as expected, our calculated binding energy for the two aliphatic compounds (ethylene and propylene) exhibits clearly different magnitude and trend than those of the aromatic compounds (Figure 2). This contrast is caused not only by the different numbers of atoms in the molecules but also by a significant difference in the surface coverage. By examining the morphology of the formed clusters, we find that most of the aromatic molecules aggregate on the NPs more readily than the aliphatic ones, as shown in Figure 3, taking the cases of toluene and ethylene for comparison. This may stem from the characteristic stacking pattern of sp^2-hybridized carbon,[37,38] through which the planar molecular structure helps to form thermally stable aggregates not only on the NP surface but also in the gas phase. This hypothesis is consistent with the observation that the bigger the NP (hence the flatter its surface), the stronger the binding energy, as shown in Figure 2. It also agrees with previous experimental results that have shown that cyclic compounds contribute much more to PM formation than linear and branched compounds.[39−41]

Our simulations reveal that, with an increasing number of adsorbates, the aromatic molecules first form a thin layer of molecules on the NP until its surface is saturated (*e.g.*, $N = 120$, middle panel of Figure 3c). Island-shaped 3D aggregates are then observed for $N = 400$, as shown in the right panel of Figure 3c. In contrast, the ethylene molecules are found to be hard to adsorb on the NP as many molecules are isolated in the gas phase. A comprehensive characterization of this behavior is shown in the Supporting Information, which contains optimized molecular configurations in which the layer-to-island nucleation behavior can clearly be observed, at room temperature, for all the studied aromatic compounds.

To quantitatively characterize the layer-to-island stacking mechanism, as shown in Figure 4, we plot the distribution of the number of molecules at different distances d from the center of mass of the NP, taking toluene and *para*-xylene as examples, as well as the stacking angle θ, defined as the angle between the normals to the molecular plane and the NP surface. It can be observed that the stacking configurations of the molecules are strongly correlated with θ. For example, the first peak in the molecular distribution shown in the green zone of Figure 4a corresponds to the first layer of adsorbed molecules, which roughly orient parallel to the NP surface as exhibited by the relatively small value of the corresponding angle θ (Figure 4b). The second peak in the distribution curve might point to a transitional layer, as shown in the yellow region of Figure 4. However, a less ordered arrangement of the molecules was observed in the second transitional layer because the standard deviation of θ is larger than that obtained for the first layer. Above these two layers, the molecules stack randomly to form 3D islands, as evidenced by the relatively large values of θ and their standard deviations in the white area, as shown in Figure 4b. We also observe the desorption of

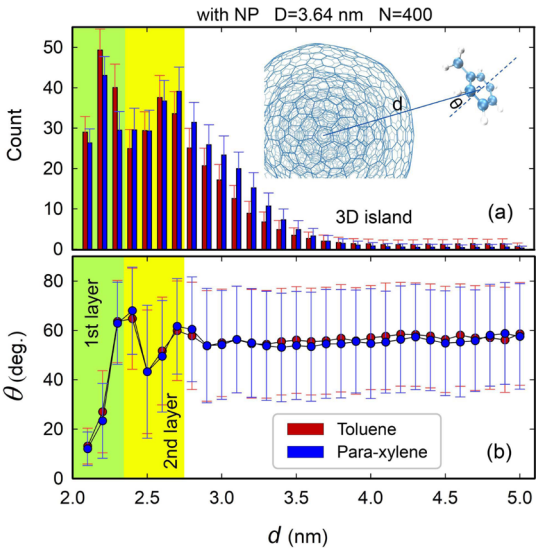

Figure 4. (a) Distribution of the numbers of adsorbed molecules at different distances d from the center of mass of the NP ($D = 3.64$ nm) for the cases of 400 toluene and *para*-xylene molecules. (b) Stacking angle θ of the 400 molecules as a function of d. The insets show how d and θ are defined. The data are averaged over the last 1000 frames of simulation for 500 ps. The error bars represent the standard deviations. Means and standard deviations are estimated over 1000 (a) and 1000 × count (b) samples, respectively.

molecules from the outermost layer. These molecules likely orient perpendicular rather than parallel to the surface before and after desorption and exhibit an average stacking angle larger than 45°.

Figure 5b,c shows that the molecules start to form aggregates approximately at a critical density of $N = 120$. This is consistent with the fact that the binding energy of the aromatic compounds (toluene, styrene, ethylbenzene, and *para*-xylene) evolves toward a different slope at this density, as shown in Figure 2a for the case of the gas phase where the

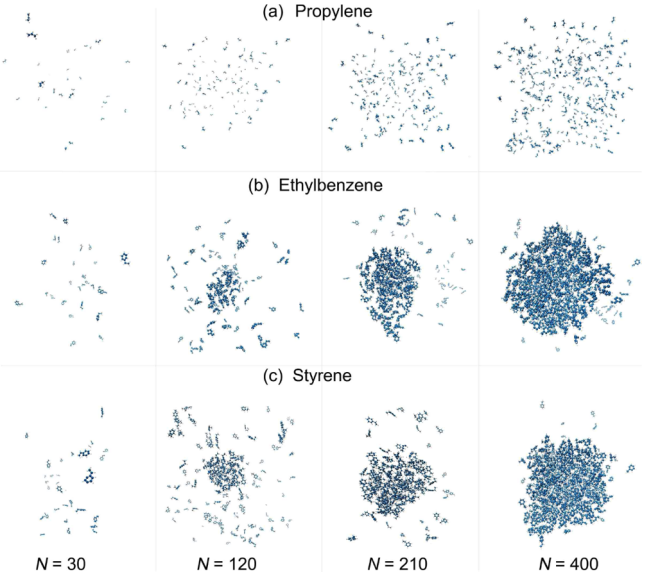

Figure 5. Atomistic configurations of different numbers of (a) propylene, (b) ethylbenzene, and (c) styrene molecules in the gas phase.

https://doi.org/10.1021/acsomega.1c03571
ACS Omega 2021, 6, 27898−27904

energy is simply a function of the molecular density. It can also be observed that the energy curves change the slope again at N = 210, where only a very small portion of molecules remains disaggregated in the pure gas phase.

Figure 6a shows the distribution of the number of molecules at different distances d from the center of mass of the aggregate

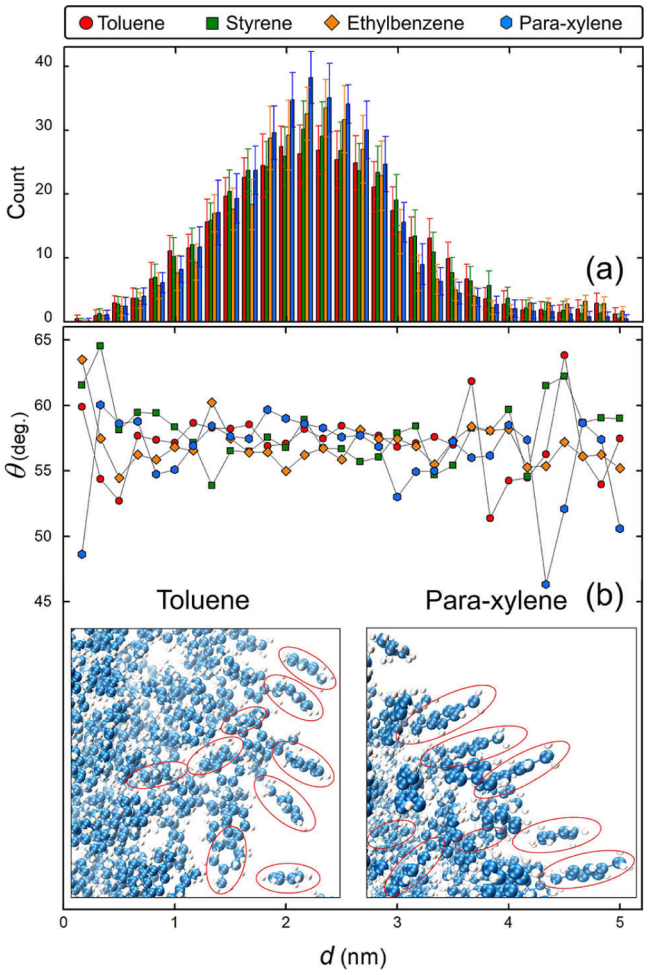

Figure 6. (a) Distribution of the numbers of molecules at different distances d from the center of mass of the aggregate of about 400 molecules formed in the gas phase. (b) Stacking angle θ of the 400 molecules as a function of d. θ is defined here in a similar fashion to what is shown in the inset of Figure 4, but the vector from the center of mass of the aggregate to that of the molecule is used instead of the surface normal. The insets show the positions of the molecules at the outermost layer of the aggregates. The data are averaged over the last 50 frames of simulation for 25 ps, considering that the translation and rotation of the clusters in the gas phase are more active than the case with the NP. The error bars represent the standard deviations. The data are estimated over 50 (a) and 50 × count (b) samples, respectively.

formed by about 400 aromatic molecules in the gas phase. It is shown that the aggregations of styrene and toluene exhibit more homogeneous spatial distributions compared with *para*-xylene and ethylbenzene molecules. This difference in the nucleation behavior of the aromatic compounds is consistent with the calculations of binding energies, as shown in Figure 2a, which may stem from the various structures of their functional groups. The different spatial arrangements could be related to the different structures of the functional groups of the aromatic molecules. More specifically, toluene and styrene molecules exhibit smaller functional groups, and it is, therefore, easier for them to find a homogeneous spatial distribution than *para*-xylene and ethylbenzene molecules. Based on the corresponding distribution of the stacking angle (>45°) shown in Figure 6b, the benzene plane tends to have a shift from being perfectly perpendicular to the radial direction, which connects the mass center of the aggregate and that of the molecule. This behavior is particularly apparent for the outermost layer of the molecular aggregates, as shown in the insets of Figure 6b.

CONCLUSIONS

Using MD, we have simulated the physisorption of ethylene, propylene, toluene, styrene, ethylbenzene, and *para*-xylene molecules on soot NPs at room temperature. The calculation of the binding energy indicates that the soot NP could help to form thermally stable molecular clusters with respect to the case in the pure gas phase. This points to a possible active role of the soot in the formation of organic PM, in general agreement with previous experimental observations. As expected, a clear difference in the nucleation behaviors was observed between the studied aromatic and aliphatic compounds (the aromatic molecules aggregated more readily than the aliphatics did). Our simulations reveal a layer-to-island nucleation mechanism: With an increasing number of the adsorbed molecules, the adsorbates first formed a thin shell on the substrate until the surface was saturated. A second transitional layer then appears before the formation of aggregates in an island shape. These findings suggest a microscopic mechanism for the formation of soot-PM by the nucleation of organic compounds on soot NPs.

ASSOCIATED CONTENT

Supporting Information

The Supporting Information is available free of charge at https://pubs.acs.org/doi/10.1021/acsomega.1c03571.

Potential energy of the system versus simulation time; time-evolution of the distribution of the adsorbed molecules; snapshots of the simulated system; detailed explanation of the data files containing molecular configurations; and set of example LAMMPS input files for simulation (ZIP)

AUTHOR INFORMATION

Corresponding Author

Yulu Zhou − *Department of Physics, Guangxi University, Nanning 530004, China;* orcid.org/0000-0002-8305-5861; Email: ylzhou@gxu.edu.cn

Authors

Xiaoqi Zhou − *Department of Physics, Guangxi University, Nanning 530004, China*

Zhisen Meng − *Department of Physics, Guangxi University, Nanning 530004, China*

Sylvain Picaud − *Institut UTINAM, CNRS UMR 6213, UBFC, 25030 Besançon, France;* orcid.org/0000-0003-1277-6466

Michel Devel − *FEMTO-ST Institute, 25030 Besançon, France*

Jesús Carrete − *Institute of Materials Chemistry, TU Wien, A-1060 Vienna, Austria;* orcid.org/0000-0003-0971-1098

https://doi.org/10.1021/acsomega.1c03571
ACS Omega 2021, 6, 27898−27904

Georg K. H. Madsen − *Institute of Materials Chemistry, TU Wien, A-1060 Vienna, Austria;* orcid.org/0000-0001-9844-9145

Zhao Wang − *Department of Physics, Guangxi University, Nanning 530004, China*

Complete contact information is available at: https://pubs.acs.org/10.1021/acsomega.1c03571

Notes

The authors declare no competing financial interest.

■ ACKNOWLEDGMENTS

P. Blaha and K. Schwarz are acknowledged for helpful discussions. Support from the National Natural Science Foundation of China (11964002) is acknowledged.

■ REFERENCES

(1) Zhang, R.; Wang, G.; Guo, S.; Zamora, M. L.; Ying, Q.; Lin, Y.; Wang, W.; Hu, M.; Wang, Y. Formation of urban fine particulate matter. *Chem. Rev.* **2015**, *115*, 3803−3855.

(2) Baldelli, A.; Trivanovic, U.; Sipkens, T. A.; Rogak, S. N. On determining soot maturity: A review of the role of microscopy-and spectroscopy-based techniques. *Chemosphere* **2020**, *252*, 126532.

(3) Nienow, A. M.; Roberts, J. T. Heterogeneous chemistry of carbon aerosols. *Annu. Rev. Phys. Chem.* **2006**, *57*, 105−128.

(4) Zhang, R.; Khalizov, A. F.; Pagels, J.; Zhang, D.; Xue, H.; McMurry, P. H. Variability in morphology, hygroscopicity, and optical properties of soot aerosols during atmospheric processing. *Proc. Natl. Acad. Sci. U.S.A.* **2008**, *105*, 10291−10296.

(5) Laskin, A.; Moffet, R. C.; Gilles, M. K. Chemical imaging of atmospheric particles. *Acc. Chem. Res.* **2019**, *52*, 3419−3431.

(6) Adachi, K.; Chung, S. H.; Buseck, P. R. Shapes of soot aerosol particles and implications for their effects on climate. *J. Geophys. Res.: Space Phys.* **2010**, *115*, D15206.

(7) Zhang, R.; Khalizov, A.; Wang, L.; Hu, M.; Xu, W. Nucleation and growth of nanoparticles in the atmosphere. *Chem. Rev.* **2012**, *112*, 1957−2011.

(8) Thanh, N. T. K.; Maclean, N.; Mahiddine, S. Mechanisms of nucleation and growth of nanoparticles in solution. *Chem. Rev.* **2014**, *114*, 7610−7630.

(9) Lazar, P.; Karlický, F.; Jurečka, P.; Kocman, M.; Otyepková, E.; Šafářová, K.; Otyepka, M. Adsorption of small organic molecules on graphene. *J. Am. Chem. Soc.* **2013**, *135*, 6372−6377.

(10) Veclani, D.; Melchior, A. Adsorption of ciprofloxacin on carbon nanotubes: Insights from molecular dynamics simulations. *J. Mol. Liq.* **2020**, *298*, 111977.

(11) Yang, K.; Zhu, L.; Xing, B. Adsorption of polycyclic aromatic hydrocarbons by carbon nanomaterials. *Environ. Sci. Technol.* **2006**, *40*, 1855−1861.

(12) Su, W.; Zhang, A.; Sun, Y.; Ran, M.; Wang, X. Adsorption properties of C2H4 and C3H6 on 11 adsorbents. *J. Chem. Eng. Data* **2017**, *62*, 417−421.

(13) Daifullah, A. A. M.; Girgis, B. S. Impact of surface characteristics of activated carbon on adsorption of BTEX. *Colloids Surf., A* **2003**, *214*, 181−193.

(14) Liu, C.-H.; Li, J.-J.; Zhang, H.-L.; Li, B.-R.; Guo, Y. Structure dependent interaction between organic dyes and carbon nanotubes. *Colloids Surf., A* **2008**, *313*−*314*, 9−12.

(15) Kragulj, M.; Tričković, J.; Dalmacija, B.; Kukovecz, Á.; Kónya, Z.; Molnar, J.; Rončević, S. Molecular interactions between organic compounds and functionally modified multiwalled carbon nanotubes. *Chem. Eng. J.* **2013**, *225*, 144−152.

(16) Li, J.-R.; Kuppler, R. J.; Zhou, H.-C. Selective gas adsorption and separation in metal−organic frameworks. *Chem. Soc. Rev.* **2009**, *38*, 1477−1504.

(17) Wu, H.; Gong, Q.; Olson, D. H.; Li, J. Commensurate adsorption of hydrocarbons and alcohols in microporous metal organic frameworks. *Chem. Rev.* **2012**, *112*, 836−868.

(18) Düren, T.; Bae, Y.-S.; Snurr, R. Q. Using molecular simulation to characterise metal−organic frameworks for adsorption applications. *Chem. Soc. Rev.* **2009**, *38*, 1237−1247.

(19) Li, J.; Posfai, M.; Hobbs, P. V.; Buseck, P. R. Individual aerosol particles from biomass burning in southern Africa: 2. Compositions and aging of inorganic particles. *J. Geophys. Res.: Atmos.* **2003**, *108*, 8484.

(20) Wentzel, M.; Gorzawski, H.; Naumann, K.-H.; Saathoff, H.; Weinbruch, S. Transmission electron microscopical and aerosol dynamical characterization of soot aerosols. *J. Aerosol Sci.* **2003**, *34*, 1347−1370.

(21) Müller, J.-O.; Su, D. S.; Wild, U.; Schlögl, R. Bulk and surface structural investigations of diesel engine soot and carbon black. *Phys. Chem. Chem. Phys.* **2007**, *9*, 4018−4025.

(22) Langlet, R.; Mayer, A.; Geuquet, N.; Amara, H.; Vandescuren, M.; Henrard, L.; Maksimenko, S.; Lambin, P. Study of the polarizability of fullerenes with a monopole-dipole interaction model. *Diamond Relat. Mater.* **2007**, *16*, 2145−2149.

(23) García Fernández, C.; Picaud, S.; Devel, M. Calculations of the mass absorption cross sections for carbonaceous nanoparticles modeling soot. *J. Quant. Spectrosc. Radiat. Transfer* **2015**, *164*, 69−81.

(24) Hsieh, C.-C.; Tsai, J.-H. VOC concentration characteristics in Southern Taiwan. *Chemosphere* **2003**, *50*, 545−556.

(25) Cao, H.; Fu, T.-M.; Zhang, L.; Henze, D. K.; Miller, C. C.; Lerot, C.; Abad, G. G.; De Smedt, I.; Zhang, Q.; van Roozendael, M.; et al. Adjoint inversion of Chinese non-methane volatile organic compound emissions using space-based observations of formaldehyde and glyoxal. *Atmos. Chem. Phys.* **2018**, *18*, 15017−15046.

(26) Plimpton, S. Fast parallel algorithms for short-range molecular dynamics. *J. Comp. Phys.* **1995**, *117*, 1−19.

(27) Stuart, S. J.; Tutein, A. B.; Harrison, J. A. A reactive potential for hydrocarbons with intermolecular interactions. *J. Chem. Phys.* **2000**, *112*, 6472−6486.

(28) Wang, Z.; Devel, M. Periodic ripples in suspended graphene. *Phys. Rev. B* **2011**, *83*, 125422.

(29) Vekeman, J.; Sánchez-Marín, J.; Sánchez de Merás, A.; Garcia Cuesta, I.; Faginas-Lago, N. Flexibility in the graphene sheet: the influence on gas adsorption from molecular dynamics studies. *J. Phys. Chem. C* **2019**, *123*, 28035−28047.

(30) Ramanathan, V.; Carmichael, G. Global and regional climate changes due to black carbon. *Nat. Geosci.* **2008**, *1*, 221−227.

(31) Trompetter, W. J.; Grange, S. K.; Davy, P. K.; Ancelet, T. Vertical and temporal variations of black carbon in New Zealand urban areas during winter. *Atmos. Environ.* **2013**, *75*, 179−187.

(32) Shen, L.; Li, L.; Lü, S.; Zhang, X.; Liu, J.; An, J.; Zhang, G.; Wu, B.; Wang, F. Characteristics of black carbon aerosol in Jiaxing, China during autumn 2013. *Particuology* **2015**, *20*, 10−15.

(33) Chen, Y.; Schleicher, N.; Fricker, M.; Cen, K.; Liu, X.-l.; Kaminski, U.; Yu, Y.; Wu, X.-f.; Norra, S. Long-term variation of black carbon and $PM_{2.5}$ in Beijing, China with respect to meteorological conditions and governmental measures. *Environ. Pollut.* **2016**, *212*, 269−278.

(34) Arif, M.; Kumar, R.; Kumar, R.; Eric, Z.; Gourav, P. Ambient black carbon, $PM_{2.5}$ and PM_{10} at Patna: Influence of anthropogenic emissions and brick kilns. *Sci. Total Environ.* **2018**, *624*, 1387−1400.

(35) Sarkar, C.; Roy, A.; Chatterjee, A.; Ghosh, S. K.; Raha, S. Factors controlling the long-term (2009-2015) trend of $PM_{2.5}$ and black carbon aerosols at eastern Himalaya, India. *Sci. Total Environ.* **2019**, *656*, 280−296.

(36) Wang, Z. Selective conduction of organic molecules via free-standing graphene. *J. Phys. Chem. C* **2019**, *123*, 15166−15170.

(37) Björk, J.; Hanke, F.; Palma, C.-A.; Samori, P.; Cecchini, M.; Persson, M. Adsorption of aromatic and anti-aromatic systems on graphene through π-π stacking. *J. Phys. Chem. Lett.* **2010**, *1*, 3407−3412.

(38) Roos, M.; Künzel, D.; Uhl, B.; Huang, H.-H.; Brandao Alves, O.; Hoster, H. E.; Gross, A.; Behm, R. J. Hierarchical interactions and their influence upon the adsorption of organic molecules on a graphene film. *J. Am. Chem. Soc.* **2011**, *133*, 9208−9211.
(39) Jiang, B.; Xia, D.; Xie, Y.; Liu, X. Effect of the molecular structure of volatile organic compounds on atmospheric nucleation: A modeling study based on gas kinetic theory and graph theory. *Atmos. Environ.* **2019**, *213*, 215−222.
(40) Haritash, A. K.; Kaushik, C. P. Biodegradation aspects of Polycyclic Aromatic Hydrocarbons (PAHs): A review. *J. Hazard. Mater.* **2009**, *169*, 1−15.
(41) Mu, L.; Peng, L.; Liu, X.; He, Q.; Bai, H.; Yan, Y.; Li, Y. Emission characteristics and size distribution of polycyclic aromatic hydrocarbons from coke production in China. *Atmos. Res.* **2017**, *197*, 113−120.

https://doi.org/10.1021/acsomega.1c03571
ACS Omega 2021, 6, 27898−27904